Astron. Astrophys. 324, 904–914 (1997)

ASTRONOMY
AND
ASTROPHYSICS

Complex variability pattern in NGC 4151

I. Sequences on the line-continuum diagram⋆

Yu.F. Malkov, V.I. Pronik, and S.G. Sergeev

Crimean Astrophysical Observatory, P/O Nauchny, 334413 Crimea, Ukraine

Received 2 August 1996 / Accepted 28 January 1997

Abstract. We present the first results of an 8-year spectroscopic monitoring of the Seyfert 1.5 galaxy NGC 4151 carried out with a CCD spectrograph at the 2.6-m Shajn Telescope of the Crimean Astrophysical Observatory in 1988-1995. Total of 202 Hα region spectra and 154 Hβ region spectra have formed the data set. All spectra were calibrated in flux using the narrow emission lines which were assumed to be constant over the duration of the monitoring program. A self-consistent seeing correction procedure not requiring the surface brightness distribution of the narrow-line region to be known is proposed. The seeing-corrected Hα, Hβ, and He II λ4686 integrated line fluxes and the optical continuum fluxes at 4480Å, 5120Å, 6230Å, and 6910Å are tabulated. During the monitoring program, the spectrum and luminosity of NGC 4151 have undergone dramatic changes. The broad-line fluxes grew by at least 4.6 times for the Hα, 6.5 times for the Hβ, and 9 times for the He II λ4686 lines whereas the non-thermal optical continuum at 5120Å increased by at least 4.8 times. The light curve of the He II λ4686 line strongly differs from the Hα and Hβ light curves. Moreover, there is a clearly pronounced, broad, variable emission near the observed wavelength 4540Å whose variations are not correlated with variations of the broad He II λ4686 line.

The line-continuum diagrams for NGC 4151 reveal some features which contradict the simplest AGN paradigm where a single central source of the continuum emission has a steady relationship between the visible and ionizing continuum:

(1) each of the dependences of Hα, Hβ, and He II λ4686 emission-line fluxes on the optical continuum flux split into four sequences which cover different periods of observations and differ by most parameters of the line-continuum and line-line correlations, including the time lag between the continuum and line variations;

(2) some sequences do not pass through the zero-point of both broad-line and non-thermal optical continuum fluxes, and the relative position of these sequences on the line-continuum diagram is quite different for the hydrogen and He II lines;

(3) the transition time between two successive sequences ($\sim$ 100 days or less) is much shorter than the dynamical time scale for the broad-line region ($\sim$ several years), so the spatial redistribution of the line-emitting gas is obviously not the cause of the origin of sequences (and, hence, of the changes in the emission-line lag).

Key words: galaxies: active – galaxies: individual: NGC 4151 – galaxies: nuclei – galaxies: Seyfert – galaxies: emission lines

1. Introduction

Our knowledge about the size, geometry, and kinematics of the broad-line region (BLR) in active galactic nuclei (AGN) is based exclusively on the analysis of variability in these objects. The correlation between the broad-line and continuum fluxes verifies both the photoionization mechanism of the gas luminescence and the link between the optical/ultraviolet and ionizing continuum. Existence of such a correlation as well as the small characteristic time of broad-line variability ($\sim$ 10 days) provide evidence for a small size of BLR. The best indicator of the BLR size is the time lag between the continuum and line variations interpreted as the light travel time effect. At present, it is certainly established that the broad-line time lag in AGNs lies in the range from several days to several tens of days, so the linear dimension of BLR is of order 0.1 pc or less.

A more detailed consideration of the response of a BLR cloud system to the continuum variations has shown that in principle it is possible to determine the BLR geometry and kinematics (Fabrika 1980a,b; Blandford & McKee 1982). This "reverberation mapping" technique is based on several fundamental assumptions (see, e.g., Peterson (1993) for a review and references). The most important of them are that the continuum emission originates in a single, small central source and that there is a simple relationship between the observable continuum and the ionizing continuum that is driving the lines. Besides, reliable conclusions about the BLR velocity field can be

Send offprint requests to: Yu.F. Malkov

⋆ Tables 1-4 and Fig. 3 are only available in electronic form at the CDS via anonymous ftp to cdsarc.u-strasbg.fr (130.79.128.5) or via http://cdsweb.u-strasbg.fr/Abstract.html

derived from the reverberation mapping studies in the only case of one-component BLR with a single type of kinematics (e.g., outflow, or rotation, or chaotic motion etc.). Otherwise, the line response to the continuum variations may be too complicated to be analyzed.

Meanwhile, some new unexpected results suggesting the multi-component structure of the BLR in the Seyfert nuclei of NGC 5548 and NGC 4151 have been obtained (Sergeev et al. 1994). It has been found that for both galaxies the relationship between the Hα or Hβ integrated line fluxes and the optical continuum flux is not linear as a whole and splits into separated sequences belonging to different periods of observations. Thus, the optical continuum light curve is not a good representation of ionizing continuum variations. Changes in the line profile variability pattern have been detected as well, again for both NGC 5548 and NGC 4151. For instance, in 1988-1991 the correlation between the line flux and the optical continuum flux was high at each wavelength in the Hα profile of NGC 4151, but in 1991-1993 there were some spots in the line profile where the correlation was very poor. This suggests the presence of at least two variable components in the broad-line profile, one of which may not correlate with optical continuum flux.

Now, we have a possibility to investigate in detail the complex variability pattern in NGC 4151 on the basis of the long-term spectral monitoring of this source carried out in the Crimean Astrophysical Observatory during 8 years. The present paper is devoted mainly to the description of observational data, light curves, and line-continuum diagrams. The variability of broad-line profiles and the behaviour of continuum at different wavelengths will be analyzed in subsequent papers.

2. Observational data

2.1. Instrumentation and data processing

In the present paper we have used CCD spectra of NGC 4151 obtained on the 2.6-m Shajn Telescope of the Crimean Astrophysical Observatory in 1988-1995. The spectra have been registered at the spectral regions near Hα and Hβ lines. In 1988-1992, we had one observational set (2-3 nights) per month. Since 1992, the observational rate has been increased to 2 sets per month.

During 1988-1991 the observations were carried out with Cassegrain focus spectrograph with 576×375 pixels Astromed-2000 CCD. The mean spectral resolution was 4.5Å, a CCD frame covered $\sim$ 800Å spectral region. The slit was aligned on right ascension (PA=90°) and its width was 2″. Hereafter, this data set is referred to as "Cassegrain spectra". The available software allowed us to obtain several one-dimensional spectra in specified extraction regions of a given image. Thus, the processing of two-dimensional images was not possible. For most observations, we have set 5-6 extraction regions followed continuously each by another. The width of a region was $\sim$ 6″, thus all regions together covered 30-36″ along the slit. As a rule, 2-3 regions were co-added to obtain the resulting spectrum of the galactic nucleus, while the rest of the regions were co-added to obtain the sky background spectrum to be subtracted from the nucleus spectrum. The spectra were corrected for the flat field obtained at the same extraction regions. The comparison spectrum of a Ne-Ar-He lamp was used for the wavelength calibration. Typical errors of wavelength calibration were about 0.1Å for the Hα-region spectra and 0.2Å for the Hβ ones. The procedure of relative flux calibration was the most difficult problem for the Cassegrain observations because too few spectra of spectrophotometric standard stars have been obtained. The Hα region spectra have been calibrated as described by Sergeev (1994). In the Hβ region, intrinsic relative intensities of 10 emission lines in the comparison spectrum of Ne-Ar-He lamp have been determined using available spectra of standard stars. Then, for each observation of NGC 4151 the observed-to-intrinsic line intensity ratios in the comparison spectrum were fitted by a low order polynom as a function of wavelength, and the observed spectrum of galaxy was divided by this polynom. Of course, the accuracy of such a procedure of relative flux calibration is not high because the atmospheric transmission is taken into account very roughly.

Since 1991 November, the observations were carried out with a spectrograph mounted in the Nasmyth focus of 2.6-m telescope. The Astro-550 CCD with size of 580×520 pixels was used. For this data set, hereafter referred to as "Nasmyth spectra", the entrance slit width has been changed from 2″.3 in 1991-1992 to 3″.0 in 1993-1995, the slit position angle was 90°, the spectral resolution was 8Å, while a CCD frame covered $\sim$1200Å. A two-dimensional image was registered, unbiased and then corrected for the flat field. We extracted the galactic nucleus spectrum, the sky background and comparison spectra (Ne-Ar-He lamp) using 11″ extraction window. The regions to extract the sky background have been selected at 14″ distance on both sides from the nucleus. The one-dimensional spectra were obtained by direct integration across the dispersion. After the spikes cleaning and wavelength calibration, the sky background spectra were averaged and subtracted from the nucleus spectrum removing the night sky emission features. CCD frames of spectrophotometric standard star 55 UMa were handled in the same way. The spectral energy distribution for this star has been taken from Kharitonov et al. (1988). As a rule, four short-time exposures of standard star per each galaxy exposure have been obtained at approximately the same zenith distance. The standard star spectra were used to remove telluric absorption features from the spectra of NGC 4151 as well as to provide the relative flux calibration.

Using the standard star, we have also measured the "seeing" defined as FWHM of the cross-dispersion profile on CCD frame. The reason to use the star instead of the nucleus itself is that during a relatively long ($\sim$ 20 min) nucleus exposure the tracking errors along the slit are greater than in across direction while during a very short standard star exposure ($\sim$ 10-15^s) these errors are comparable.

2.2. Calibration and measurements of spectra

The absolute calibration of obtained spectra was based on the narrow-line fluxes which were assumed to be constant over

the duration of the monitoring program. In the Hβ region, the [O III] λ5007 narrow emission line was chosen as the calibrator. The flux in this line was measured in each spectrum between the observed wavelengths 4995-5055Å by summing the flux above a straight line passing between the average flux in the continuum zones 4465-4495, 5095-5140Å for Nasmyth spectra and 4770-4783, 5095-5140Å for Cassegrain spectra (see below about the choice of these zones; the effect of weak narrow lines in the continuum zones on the [O III] λ5007 flux measurements is definitely negligible). Then, all Hβ region spectra have been scaled to the same [O III] λ5007 flux of $1.14 \times 10^{-11}\ ergs\,cm^{-2}\,s^{-1}$(hereafter, all fluxes are given in observer's frame). This value has been obtained in 1992 on photometric nights using the spectrophotometric standard star 55 UMa; it is consistent with the Antonucci & Cohen (1983) result of $(1.19 \pm 0.06) \times 10^{-11}\ ergs\,cm^{-2}\,s^{-1}$.

The [S II] $\lambda\lambda$6717,6731 and [O I] λ6300 lines are the most suitable flux calibrators in the Hα region. Unfortunately, these lines are situated on the far wings of the variable broad Hα line, and variations of Hα wings will affect direct measurements of [S II] and [O I] fluxes. Therefore, another scaling method was used in this case. A spectrum with the best spectral resolution and good signal-to-noise ratio was chosen as the reference spectrum. The scaling factor, wavelength shift, and convolution parameter ΔW were then found for each Hα region spectrum by minimizing the narrow-line residuals in the difference between this spectrum and the reference spectrum convolved with a Gaussian profile of width ΔW. The narrow-line zones where the residuals were minimized were 6305-6342Å (observed wavelengths) for the [O I] λ6300 line and 6724-6770Å for the [S II] $\lambda\lambda$6717,6731 lines. As a result, we had an internally calibrated set of spectra with adjusted flux scale, spectral resolution, and wavelength scale. The absolute calibration has been achieved by comparing the spectra of NGC 4151 and 55 UMa obtained on photometric nights in 1992.

The spectral resolution and wavelength scale of Hβ region spectra have been adjusted using the [O III] λ5007 line by the same way as for the Hα region spectra.

Total of 103 Cassegrain spectra (79 in the Hα region and 24 in the Hβ region) and 253 Nasmyth spectra (123 and 130 respectively) have formed the final data set. In order to improve the data quality, all spectra have been nightly averaged. The first two columns of Tables 1-4 give the average Julian Date for a night and the number of averaged individual spectra. The average seeing measured as described in Sect.2.1 is given in the third column of Tables 3 and 4. Figs. 1 and 2 illustrate the long-term spectral variability of NGC 4151 in order to make clear our choice of the line and continuum zones. All spectra are shown on the same flux scale, without any vertical shift.

Mean Hβ region spectra of NGC 4151 at different epochs are displayed in Fig. 1. All individual spectra have been averaged in the time intervals JD 2447270-7977, 8742-9191, 9311-9313, and 9813-9891. Seven spectra with highest state of He II λ4686 line have been selected from the time interval JD 2449519-9691 and averaged into a spectrum shown in Fig. 1. Two continuum zones (observed wavelengths 4465-4495Å and

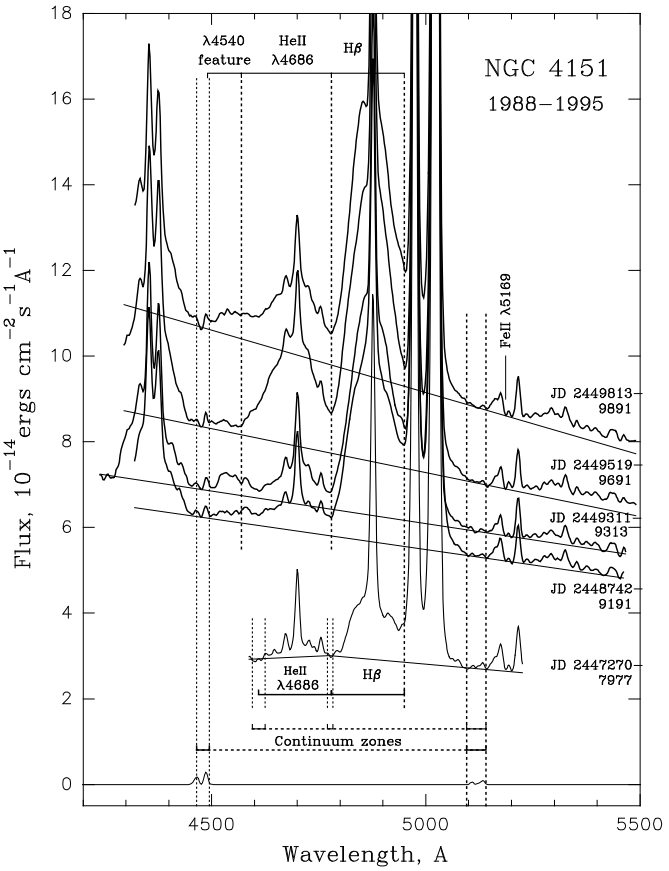

Fig. 1. Mean Hβ region spectra of NGC 4151 at different epochs (see text for explanations). All spectra are shown on the same flux scale without any vertical shift. Flux and wavelengths are given in observer's frame. The position of the Fe II λ5169 (m42) line is marked in order to emphasize the absence of any variable emission at this wavelength.

5095-5140Å) have been chosen for Nasmyth Hβ region spectra. It is clearly seen from Fig. 1 that this is the uniquely possible choice. Note also that *all* weak features with FWHM $\sim$10Å in Fig. 1 are weak narrow lines but not the noise. Four of them (the strongest is He I λ4471) fall into the continuum windows. These four narrow lines approximately extracted from the mean low-state Nasmyth spectrum (JD 2448742-9191) are shown separately at the bottom of Fig. 1. They were subtracted from each Hβ spectrum before continuum fitting and measuring the line and continuum fluxes. The continuum flux in each zone (F_λ(4480Å) and F_λ(5120Å)) was measured by simple flux averaging in the continuum zones. As Cassegrain spectra cover shorter wavelength range, the continuum flux was measured in only one zone (5095-5140Å), again after subtraction of two weak narrow lines.

To measure the line fluxes, the underlying continuum in the Hβ Nasmyth spectra was fitted by a straight line passing between the average flux in the continuum zones 4465-4495Å and 5095-5140Å. The JD 2449311-9313 mean spectrum (Fig. 1) obtained with a slightly different grate angle shows that this way of continuum fitting remains correct near the Hγ line in

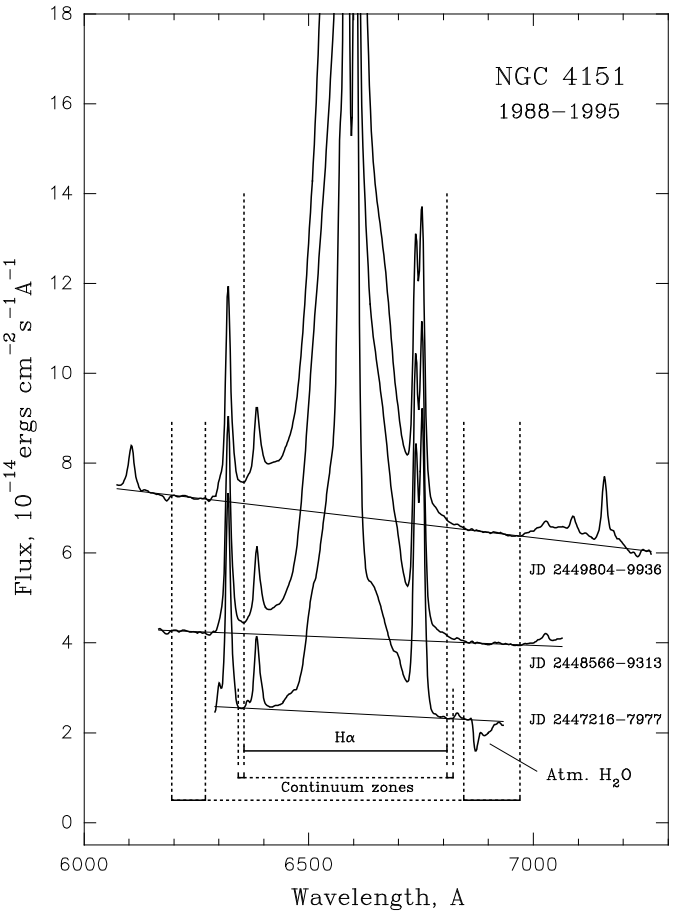

Fig. 2. The same as in Fig. 1 but for the Hα region.

the case only when the above mentioned weak narrow lines are subtracted. Note that there is a clearly pronounced, broad, variable emission feature near the observed wavelength 4540Å. Despite the fact that its variations are not correlated with variations of broad He II λ4686 line (see Fig. 5 below), we believe this feature is the very far blue wing of the He II λ4686 line (radial velocities $\sim$ 10000 km s^{-1}). The only alternative identification might be the Fe II multiplets 37 and 38 (Moore 1945) but it is clearly seen from Fig. 1 that there is no trace of *variable* Fe II λ5169 (m42) emission (5186Å in observer's frame) whose intensity in Fe II-rich AGNs is comparable to the m37 and m38 blend (Phillips 1978; Sergeev et al. 1997). The flux in the λ4540 feature was measured by summing the flux above the underlying continuum between the observed wavelengths 4490-4570Å. The He II λ4686 and Hβ fluxes in the Nasmyth spectra were integrated in the intervals 4570-4780Å and 4780-4950Å respectively (observed wavelengths). Unfortunately, the Cassegrain spectra do not cover the wavelengths shorter than $\sim$4600Å, and most of individual spectra have high noise near the blue end. In order to eliminate the effect of this noise on the Hβ flux measurements, the Hβ flux in Cassegrain spectra was measured between the observed wavelengths 4780-4950Å by summing the flux above a straight line passing between the average flux in the intervals 4770-4783Å and 5095-5140Å, whereas for the He II λ4686 flux the corresponding intervals were 4610-4780Å, 4595-4625Å, and 4770-4783Å (see Fig. 1). Possible systematic errors introduced by such a choice of wavelength intervals have been estimated by measuring the lowest state Nasmyth spectra using Cassegrain intervals. This results in no more than 7% systematic underestimate in the Hβ flux, but a possible error in the He II λ4686 flux may reach 50%. So, He II λ4686 flux measurements in the Cassegrain spectra must be considered as uncertain. The He II λ4686 line in the spectra obtained on JD 2447218, 7301, and 7645 is too noisy to be measured. Due to the same cause, the flux in the λ4540 feature was not measured in the spectra obtained on JD 2448631 and 8717.

In Fig. 2, all individual Hα region spectra have been averaged in the time intervals JD 2447216-7977, 8566-9313, 9804-9936. Two continuum zones (observed wavelengths 6195-6270Å and 6845-6970Å) have been chosen for Nasmyth spectra. There are no significant narrow lines in these zones. The continuum fluxes (F_λ(6230) and F_λ(6910)) were measured by simple flux averaging in the continuum zones. Because Cassegrain spectra cover shorter wavelength range and telluric features (H_2O absorption and night sky emission lines) have not been removed from them, the continuum zones for Cassegrain spectra have been chosen as 6343-6356Å and 6808-6821Å (Fig. 2).

The underlying continuum in Hα spectra was fitted by a straight line passing between the average flux in the continuum zones. The Hα flux in both Cassegrain and Nasmyth spectra was measured by summing the flux above the underlying continuum between the observed wavelengths 6356-6808Å. The Hα flux measured in Cassegrain spectra may be underestimated by less than 3% due to continuum zones situated on the far wings of Hα line (the error estimate has been obtained as described above for Hβ region spectra).

2.3. Correction for seeing effects

Observations made with the Hubble Space Telescope (HST) have shown that the narrow-line region (NLR) of NGC 4151 is spatially resolved, with a biconical structure spreading up to 2″ from the central source (Evans et al. 1993). The size of the extended narrow-line region (ENLR) of low surface brightness is still larger (Perez et al. 1989). Because the slit width in our observations was 3″ (or even 2″), the measured ratio of the broad-line flux (coming from a point-like source) to the narrow-line flux (emitted by a spatially extended region) depends on the seeing, and the measurements of spectra calibrated under assumption of constant narrow-line flux must be corrected for seeing effects. Unfortunately, the seeing conditions were not registered in Cassegrain observations, therefore the seeing correction procedure can be applied to Nasmyth flux measurements only.

The most straightforward way of seeing correction requires the surface brightness distribution of the NLR to be known (Wanders et al. 1992, 1993). The distribution of [O III] λ5007 surface brightness in NGC 4151 has been obtained with HST (Evans et al. 1993) while there are no such measurements for

[S II] $\lambda\lambda$6717,6731 and [O I] λ6300 lines used as the flux calibrators in our Hα region spectra. Nevertheless, the large total number of our observations allows us to develop a self-consistent seeing correction procedure without knowledge of the surface brightness distribution.

From the mathematical point of view, this procedure is very similar to the one used by Peterson et al. (1991) to intercalibrate the spectral data obtained by different observers through different apertures. Now, different seeing values play the role of different observers, and for a seeing s we can write:

$$F_{corr} = \varphi(s) \cdot F_{obs} - G(s) \quad . \tag{1}$$

Here F_{obs} and F_{corr} are the "observed" (i.e. measured from a spectrum calibrated as described in Sect.2.2) and seeing-corrected fluxes, the point-source correction factor $\varphi(s)$ accounts for the different light loss for the point-spread function and the spatially extended NLR, and the additive term $G(s)$ is the extended source correction. Evidently, for the flux from a point-like source (e.g., broad-line flux) the term $G(s)$ disappears:

$$F(point\text{-}like)_{corr} = \varphi(s) \cdot F(point\text{-}like)_{obs} \quad . \tag{2}$$

In practice, we have divided the full range of seeing values into several intervals (bins). Five seeing bins have been chosen for the Hα observations (1″.0-2″.0; 2″.0-3″.5; 3″.5-5″.0; 5″.0-6″.5; 6″.5-8″.0) and four bins for the Hβ ones (1″.0-2″.0; 2″.0-3″.5; 3″.5-7″.0; 7″.0-10″.0). The greater number of bins in the first case is caused by higher sensitivity of Hα region calibration to the seeing effects (see below). Then, each of the available spectra has been attributed to its respective seeing bin according to the seeing values listed in Tables 3 and 4. Thus, for each of the measured species (namely F$_\lambda$(4480Å), F$_\lambda$(5120Å), F(He II), F(Hβ), F(λ4540 feature), F$_\lambda$(6230Å), F$_\lambda$(6910Å), F(Hα)) we had five data sets ("pseudo-observers") in the Hα region and four in the Hβ region. Because the mean seeing at 2.6-m telescope of Crimean Observatory is 2″.8, second data set (seeing bin 2″.0-3″.5) was taken as standard in both spectral regions, and the rest of data sets were reduced to this standard by means of the procedure described in detail by Peterson et al. (1991). First, the values of $\varphi(s)$ and their formal uncertainties have been found by comparing pairs of nearly simultaneous (separated by 2 days or less) observations from different data sets (Eq.2). For the standard data set, the value φ(2″.0-3″.5)=1.00 has been adopted. The flux in Hα (Hβ) broad wings integrated from the radial velocity -4300 to -2000 km s^{-1} and from 2000 to 4300 km s^{-1} was used as the point-like source flux in (2) (the underlying continuum was subtracted as described in Sect.2.2). Then, the extended source corrections $G(s)$ and their formal uncertainties have been found for each of measured species adopting the value G(2″.0-3″.5)=0.00 for the standard data set (Eq.1).

The results are shown in Fig. 3. It is easy to see from the values of $\varphi(s)$ that the calibration in Hα region is clearly more sensitive to seeing effects than the calibration in Hβ region. The explanation is the Hα region spectra are calibrated using [O I] λ6300 and [S II] $\lambda\lambda$6717,6731 lines whose ionization potentials and critical densities are lower and, therefore, the line-emitting region is more extended than the region emitting [O III] λ5007 line used as calibrator for Hβ spectra. As expected, the values of G for the integrated Hβ flux are equal to zero within uncertainties because nearly all Hβ flux is emitted by a point-like source (BLR and inner NLR). The values of G for both F(He II) and F(λ4540 feature) (not plotted in Fig. 3) are equal to zero as well. On the contrary, $G(s)$ for the integrated Hα flux differs from zero because the integration range (see Fig. 2) includes the forbidden lines [O I] λ6364, [N II] $\lambda\lambda$6548,6584, and [S II] $\lambda\lambda$6717,6731 partially emitted by spatially extended outer NLR. Evidently, all of the continuum bands are contaminated by the host galaxy starlight and have non-zero $G(s)$.

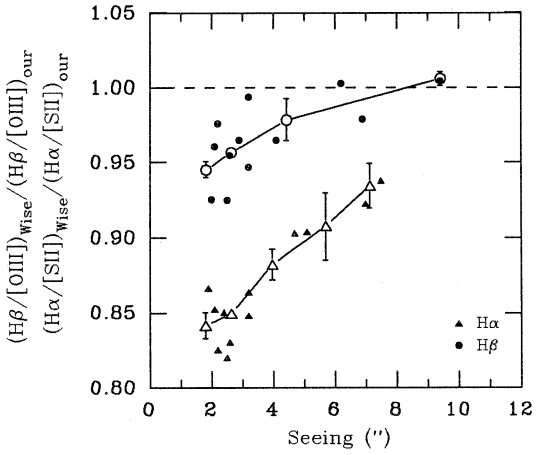

Fig. 4. Comparison of permitted-to-forbidden line ratios in Wise and our spectra (see text).

Fig. 4 provides a verification of our determination of $\varphi(s)$. During the period JD 2449305-9404, NGC 4151 was observed in Wise Observatory through a large (10″x13″) spectrograph entrance aperture with seeing from 2″ to 3″ (Kaspi et al. 1996). So far as such a large aperture covers practically the entire NLR, the flux ratios Hβ/[O III] $\lambda\lambda$4959,5007 and Hα/[S II] $\lambda\lambda$6717,6731 measured in Wise spectra must not depend on the seeing, whereas in our spectra these ratios are seeing-dependent. We have linearly interpolated the Hα and Hβ lightcurves from Kaspi et al. (1996) on the moments of our observations and then compared the Hβ/[O III] and Hα/[S II] ratios in Wise and our spectra. To do this comparison, the Hα, Hβ, and [O III] fluxes were measured in our spectra in just the same way as described by Kaspi et al. (1996). We measured the [S II] flux between the observed wavelengths 6720-6775Å by summing the flux above a straight line passing between the average flux in the intervals 6715-6720Å and 6775-6780Å. The mean [S II] flux in Wise spectra measured in the same way has been kindly provided by Dr. S.Kaspi. The seeing-dependent ratios (Hβ/[OIII])$_{Wise}$ / (Hβ/[OIII])$_{our}$ and (Hα/[S II])$_{Wise}$ / (Hα/[S II])$_{our}$ are plotted in Fig. 4 together with $\varphi(s)$ from Fig. 3 multiplied by 0.957 and 0.850 for the Hβ and Hα regions respectively in order to renormalize $\varphi(s)$. It is seen that the magnitudes of seeing effects and seeing correc-

tions are in nice agreement. As could be expected, the seeing-dependent ratios in Fig. 4 approach 1.00 at bad seeing because the point-like and extended sources become similarly blurred. Beginning from 8″ seeing, the blurred extended region emitting the [O III] λ5007 line looks like a blurred point-like source, whereas an extremely bad seeing of 11-12″ or worse is needed to blur out the [S II] line-emitting region.

The above mentioned factors 0.957 and 0.850 means that at our mean seeing of 2″.8 more than 4.3% of total [O III] λ5007 flux and more than 15% of total [S II] $\lambda\lambda$6717,6731 flux do not entered our 3″ slit. The seeing effects are thus the main source of errors in our Hα measurements. Fortunately, these effects can be taken into account, and the procedure of seeing correction significantly decrease the point-to-point scattering in the Hα lightcurve (from 3.7% to 2.8% in a 1.5 days window).

Seeing-corrected Nasmyth fluxes are given in Tables 3 and 4. Since they have been reduced to the mean seeing at 2.6-m telescope which is believed to be constant, there must be no systematic difference caused by seeing effects between Nasmyth and (uncorrected) Cassegrain fluxes. However, a systematic difference can arise due to different slit width in Cassegrain and Nasmyth observations (2″ and 3″ respectively). The NLR in NGC 4151 is spatially resolved, hence the broad-line to narrow-line flux ratio in an observed spectrum is higher when the slit is narrower. An observational experiment performed with Nasmyth spectrograph in 1996 has shown that changing the slit width from 3″ to 2″ leads to overestimating the scaling factor by 2.2% in the Hβ region and 4.3% in the Hα region. Because at the same time Cassegrain line fluxes are underestimated due to the improper choice of continuum zones (see above), a possible systematic error in the Hα fluxes in Table 1 is 1-3% overestimate whereas the Hβ fluxes in Table 2 may be systematically underestimated by up to 5%. As to the continuum fluxes derived from Cassegrain observations, they must be overestimated due to the scaling factor error as described above but at the same time they must be underestimated because the stellar contribution from the host galaxy decreases when the slit is narrower. Thus, Cassegrain and Nasmyth continuum fluxes are expected to be practically on the same scale.

3. Sequences on the line-continuum diagram

3.1. Light curves

Light curves for the emission lines and optical continuum of NGC 4151 are presented in Fig. 5. The mean accuracy of an individual flux measurement ($\pm 1\sigma$) is shown in the upper left corner of each panel. The accuracy has been estimated from the point-to-point scattering in light curves in a 1.5 day window (Table 5). Due to the lower state of nuclear activity as well as to the impossibility of seeing correction, the accuracy of Cassegrain data is somewhat lower than the mean accuracy.

Integrated Hα, Hβ, and He II λ4686 line fluxes given in Tables 1-4 and in Fig. 5 contain constant contributions from the narrow lines. We have estimated these contributions in a way described by Sergeev (1994). The resulting values are $1.0 \times 10^{-11}\ ergs\,cm^{-2}\,s^{-1}$ for the sum of narrow Hα+ [O I] λ6364+ [N II] $\lambda\lambda$6548,6584+ [S II] $\lambda\lambda$6717,6731+ narrow He I λ6678 (the value of $6.9 \times 10^{-12}\ ergs\,cm^{-2}\,s^{-1}$ given by Sergeev (1994) covers the narrow Hα+ [N II] $\lambda\lambda$6548,6584 only), $1.1 \times 10^{-12}\ ergs\,cm^{-2}\,s^{-1}$ for the narrow Hβ+ the far blue wing of [O III] λ4959, and $4.0 \times 10^{-13}\ ergs\,cm^{-2}\,s^{-1}$for the sum of narrow He II λ4686+ [Fe III] λ4658+ [Ar IV] $\lambda\lambda$4711,4740+ [Ne IV] $\lambda\lambda$4715,4725. They are shown in Fig. 5 by horizontal dashed lines. The accuracy of these estimates is not worse than 10%. Note, however, that the contribution from the narrow lines provides only a lower limit for the total constant contribution because there may be some non-variable broad emission similar to that found in Mrk 590 (Ferland et al. 1990).

Table 5. Mean accuracy (1 σ) of an individual flux measurement

Flux	Absolute accuracy	Relative accuracy
	($10^{-13} ergs\,cm^{-2}\,s^{-1}$)	
F(Hα)	5.5	1.9%
F(Hβ)	1.4	2.5%
F(He II λ4686)	1.5	9.8%
F(λ4540 feature)*	0.41	33.7%
	($10^{-15} ergs\,cm^{-2}\,s^{-1}$ Å^{-1})	
F_λ(4480Å)*	2.0	2.8%
F_λ(5120Å)	1.3	2.5%
F_λ(6230Å),F_λ(6350Å)	1.3	3.1%
F_λ(6815Å),F_λ(6910Å)	1.1	2.4%

*) Nasmyth data only

The optical continuum fluxes given in Tables 1-4 and in Fig. 5 have constant contributions due to the starlight of the host galaxy. It is known that the stellar population in Seyfert galaxies is fairly red, so the stellar contribution in U-band ($\lambda \sim$ 3600Å) is much lower than at 5120Å. The U-band fluxes derived from photometric observations of Lyutyi (1997) show a good correlation with our measurements of the continuum flux at 5120Å (the correlation coefficient is 0.984 for the pairs of observations separated by up to 1.5 day). The linear regression between these fluxes gives F^*_λ(5120Å)= $(6.1 \pm 1.5) \times 10^{-15}$ $ergs\,cm^{-2}\,s^{-1}$ Å^{-1} when the U-band flux is extrapolated to zero. Of course, this value is an absolute lower limit of stellar contribution into the continuum flux at 5120Å because the stellar flux at 3600Å is definitely present and the 27″ aperture used by Lyutyi (1997) is much larger than our 3″× 11″ aperture. A more realistic estimate of F^*_λ(5120Å) can be obtained using the linear regression between the continuum flux and the flux in a broad line (Hα, Hβ, or He II λ4686) during the low state of activity of NGC 4151 in 1988-1991. These three lines give the weighted mean value of F^*_λ(5120Å)= $(10.0 \pm 1.2) \times 10^{-15}$ $ergs\,cm^{-2}\,s^{-1}$ Å^{-1} when the broad-line flux (i.e., the integrated line flux minus the narrow-line contribution) is extrapolated to zero. This value, however, must be considered with cau-

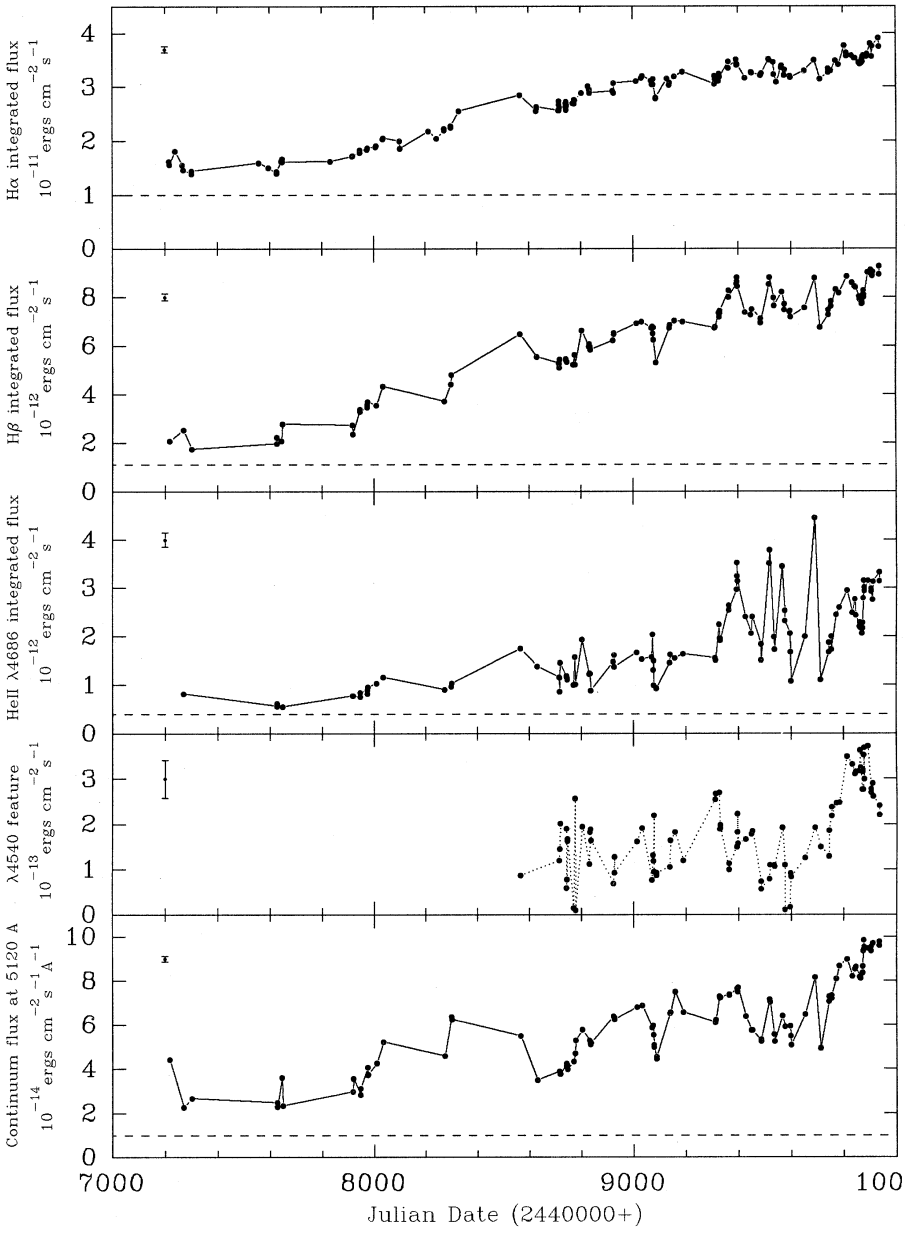

Fig. 5. Light curves for the emission lines and optical continuum of NGC 4151 in 1988-1995. Estimated constant contributions from the narrow lines and from the starlight of the host galaxy are shown by horizontal dashed lines (they were not subtracted from the light curves). The mean accuracy of an individual measurement ($\pm 1\sigma$) is shown in the upper left corner of each panel.

tion because it is not known whether the 1988-1991 sequence on the line-continuum diagram (see Fig. 8 below) went indeed through the zero-point of both broad-line and non-thermal optical continuum fluxes.

The gradual increase of flux is a general property of all light curves in Fig. 5 except, maybe, the λ4540 feature. Taking into account the constant contributions determined above, the broad-line fluxes grew from JD 2447200-7800 to JD 2449740-9940 by at least 4.6 times for the Hα, 6.5 times for the Hβ, and 9 times for the He II λ4686 lines whereas the variable part of the optical continuum at 5120Å increased by at least 4.8 times. In 1995 the nucleus of NGC 4151 has reached its historical peak brightness, both the ultraviolet data (Kriss et al. 1995) and the optical photometry (Lyutyi, private communication) confirm this conclusion.

Numerous short-term (50-100 days long) events superposed on the general flux increase are clearly pronounced on the emission-line and continuum light curves. These events appear to be concurrent on the Hα, Hβ, He II λ4686, and optical continuum light curves whereas the presence of such events on the light curve of the λ4540 feature is doubtful (the amplitude of most of them does not exceed 2σ error bar). Note the extremely high amplitude of short-term He II λ4686 flux variations during the time interval JD 2449400-9700. This strange phenomenon will be clearly seen below on the line-continuum diagram.

3.2. Line-continuum diagrams

The correlation between the broad-line and optical continuum fluxes is one of the principal observational results concerning the active galactic nuclei. During the last 25 years, such a cor-

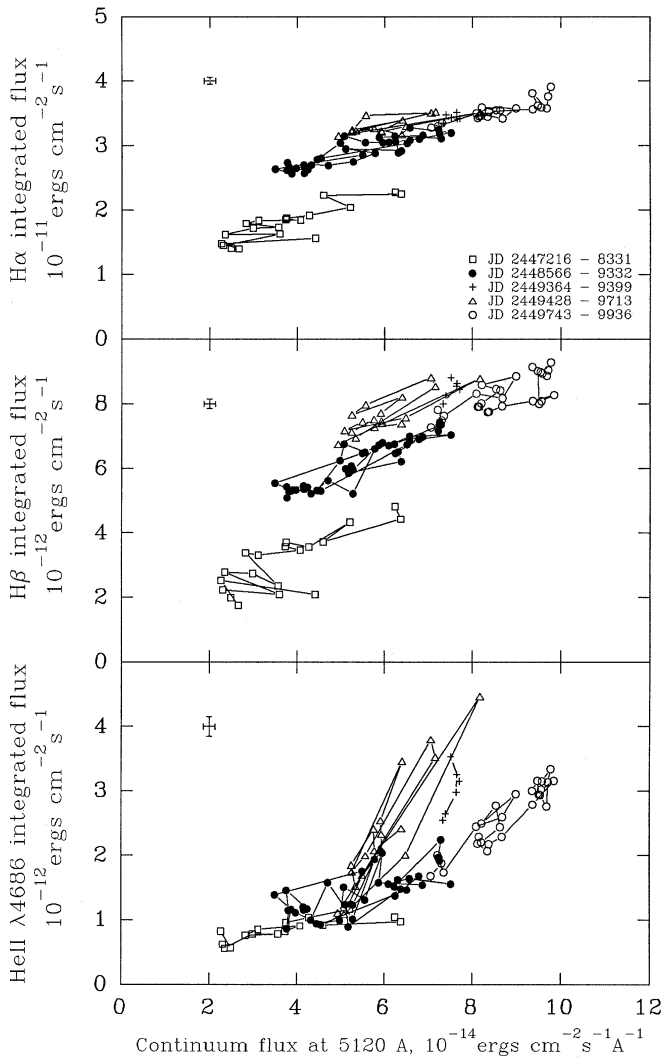

Fig. 6. Line-continuum diagrams for NGC 4151. The time lag between the continuum and line variations is not taken into account. Each point in the plot represents the continuum and line fluxes measured on the same night, so no interpolation errors are introduced. Constant contributions are not subtracted from the line and continuum fluxes. The error bars in the upper left corner mean the same as in Fig. 5. Four sequences which can be distinguished are shown by open squares, filled circles, open triangles, and open circles respectively. The transitional points between the second and third sequences are plotted as crosses.

relation has been discovered in many AGNs, and the cross-correlation technique has become widely applied to the investigations of these objects. Surprisingly, in 1993 we have found that for NGC 4151 the relationship between the Hα (Hβ) and optical continuum fluxes splits into two clearly separated, nearly parallel sequences belonging to different periods of observations (Sergeev et al. 1994). Unfortunately, the first of these periods corresponded to the Cassegrain observations but the second to Nasmyth ones, i.e. the instrumental settings were different. Some doubts about the origin of sequences remained therefore, though another Seyfert galaxy NGC 5548 observed by the International AGN Watch consortium had shown similar (but less pronounced) sequences (Sergeev et al. 1994).

Now, the line-continuum diagrams for NGC 4151 look as plotted in Fig. 6. It is clearly seen that a joint examination of all three diagrams allows us to outline the following four sequences:

I. JD 2447216-8331. The sequence is best separated on the Hα-continuum and Hβ-continuum diagrams though the He II λ4686 fluxes were the lowest as well. This sequence includes all of the Cassegrain observations (and only them). It is not known when the first sequence began really (before JD 2447216), and the transition from this sequence to the next one has not been observed because the observations were interrupted during JD 2448331-8566.

II. JD 2448566-9332. Exact date of the beginning of this sequence is not known but its end is well-defined: since JD 2449332, the Hβ and especially He II λ4686 fluxes grew rapidly while only a small and slow increase of the continuum flux at 5120Å took place (Fig. 5,6). The line-continuum correlation reappeared after JD 2449399 when the third sequence started. Therefore, the observations made on JD 2449364-9399 correspond to the transition from the second to third sequence, and the transition time was about 70 days. The second sequence contains Nasmyth observations only but they are slightly inhomogeneous so far as the slit width was changed from 2″.3 to 3″.0 between JD 2448927 and 2449014. However, the effect of such a change is not visible in Fig. 6: there is no extra splitting within the second sequence.

III. JD 2449428-9713. The most remarkable and perhaps the shortest sequence. It is nearly parallel to the second sequence on the Hα-continuum and Hβ-continuum diagrams but at the same time the amplitude of the He II λ4686 flux variations is much larger and the He II-continuum relationship goes much steeper than at any other sequence. Mean high-state spectrum of NGC 4151 at third sequence shown in Fig. 1 emphasizes the very strong emission in the He II λ4686 line.

IV. JD 2449743-9936 (and later). This sequence looks like an extension of the second sequence on the Hα-continuum and Hβ-continuum diagrams but the slope of the He II-continuum relationship is steeper than at the second sequence. The transition from third to fourth sequence was very rapid, no more than 30 days long. The true end of the fourth sequence is not observed yet.

We would to emphasize that the sequences II-IV are formed by homogeneously processed, seeing-corrected Nasmyth observations, so any instrumental effect cannot be the cause of the origin of the sequences.

It is important to note that the time lag between the continuum and line variations has not been taken into account in Fig. 6. To determine the lag more accurately, we have collected from various sources the data about the behaviour of the optical continuum of NGC 4151 in order to maximize the temporal resolution in the continuum light curve. Both spectral and photometric data were used, namely the contin-

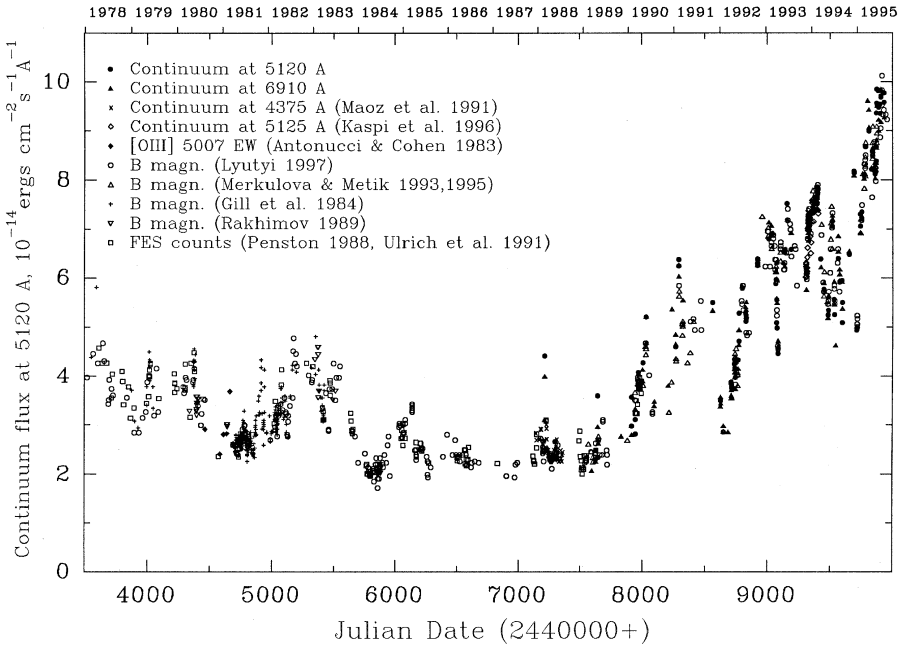

Fig. 7. Light curve for the optical continuum of NGC 4151 since 1978 formed by the intercalibration of spectral and photometric data from various sources to our instrumental system.

Table 6. Cross-correlation results

Sequence	Balmer lines			He II λ4686 line		
	τ_{peak}	τ_{centr}	r_{max}	τ_{peak}	τ_{centr}	r_{max}
I	$10^d.1 \pm 1^d.6$	$11^d.8$	0.95	–	–	0.79
II	4.8 ± 1.7	8.5	0.96	$0^d.0 \pm 1^d.7$	$0^d.5$	0.72
III	1.5 ± 1.4	2.5	0.84	0.0 ± 1.9	2.0	0.94
IV	5.2 ± 1.6	8.8	0.87	0.6 ± 1.3	2.6	0.94

uum fluxes at 6815Å and 6910Å (Tables 1 and 3), the continuum fluxes at 4375Å (Maoz et al. 1991), the continuum fluxes at 5125Å (Kaspi et al. 1996), the [O III] λ5007 equivalent widths (Antonucci & Cohen 1983), the B-magnitudes (Lyutyi 1997; Merkulova & Metik 1993, 1995, and unpublished data; Gill et al. 1984; Rakhimov 1989), and the optical flux measurements obtained with FES (Fine Error Sensor) at the IUE satellite (Penston 1988; Ulrich et al. 1991). All these data have been recalculated into our scale of continuum flux at 5120Å by means of the intercalibration procedure described in detail by Peterson et al. (1991), Korista et al. (1995), and Sergeev et al. (1997). In most cases, this procedure consisted in finding a linear regression between two series of flux measurements by comparing the pairs of nearly simultaneous observations (separated by up to several days). The resulting light curve of the continuum at 5120Å beginning in 1978 (i.e. since the IUE launch) is shown in Fig. 7. It contains 1264 measurements.

So far as the relationship between the line and continuum fluxes is divided into four sequences, we determined the lag for each sequence separately. The partial interpolation cross-correlation technique described by Gaskell & Peterson (1987) was used. The cross-correlation functions (CCF) have been calculated for the Hα, Hβ, and He II λ4686 lines. The lag values obtained for the Hα and Hβ lines have been averaged into a value representative for the region emitting the Balmer lines of hydrogen. As it can be seen from Fig. 5, the He II λ4686 light curve at the first sequence is undersampled, and the Hα and Hβ light curves are only marginally suitable for the lag determination. To find the Balmer line lag at the first sequence more reliably, we used our data in conjunction with Hα and Hβ fluxes measured by Maoz et al. (1991) on JD 2447145-7360. To join the light curves, we simply remeasured our spectra using the wavelength intervals for the Hα and Hβ integration from Maoz et al. (1991). This resulted in no systematic difference in flux between the two data sets while the r.m.s. deviation in pairs of nearly simultaneous measurements was 4.2% for the Hα and 23% for the Hβ line (the latter is determined using three pairs of observations only). Cross-correlation results for all sequences are given in Table 6 where τ_{peak} is the CCF peak position, τ_{centr} is the value of the CCF centroid which is computed using all points near the CCF peak with amplitudes greater than $0.5r_{max}$, and r_{max} is the maximal correlation at the CCF peak. As could be expected, the Balmer line lag at the first sequence has proved to be close to the value of 9$\pm$2 days found by Maoz et al. (1991) because their data constitute more than one half of the total number of measurements in the merged light curves. The uncertainties in τ_{peak} have been roughly estimated using an analytic formula suggested by Gaskell & Peterson (1987). Uncertainties in τ_{centr} are expected to be of the same order.

Despite the fact that the lag uncertainties listed in Table 6 may be underestimated, the changes of the Balmer line lag from one sequence to another are obvious. Note that Kaspi et al. (1996) have found the Hα lag of 0-2 days and the Hβ lag of 0-3 days on JD 2449305-9404 (i.e. during the transition from second to third sequence), so the small lag at third sequence is confirmed by their data. Unfortunately, the temporal resolution of our monitoring does not allow us to investigate whether the lag varies within a sequence. At all sequences, the He II λ4686 line

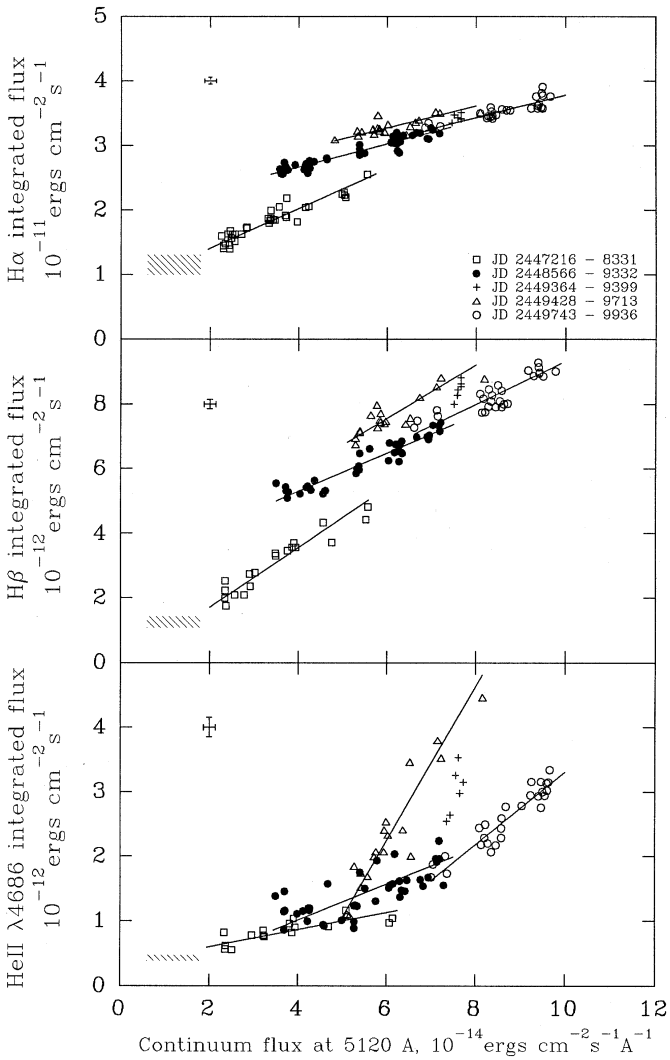

Fig. 8. Line-continuum diagrams for NGC 4151 after the emission-line lag was taken into account separately for each sequence. The continuum fluxes were obtained from the combined light curve (Fig. 7). The linear fit found with aid of the "doubly weighted" regression technique is shown for each sequence. The hatched rectangles represent the allowed area for the constant contributions in the line and continuum fluxes. Other symbols are as in Fig. 6.

responds to continuum variations more rapidly than the Balmer lines of hydrogen. Such an ionization stratification is observed in other Seyfert nuclei (Clavel et al. 1991; Dietrich et al. 1993; Reichert et al. 1994).

Having the optical continuum light curve with good temporal resolution (Fig. 7) and taking into account the emission line lags (Table 6), we have constructed in Fig. 8 the final version of the line-continuum diagrams for NGC 4151. A comparison with Fig. 6 shows that the sequences become better pronounced when the lag is accounted for, hence the light-travel time effects are not responsible for the origin of sequences in Fig. 6. We approximated each sequence in Fig. 8 by a straight line using the "doubly weighted" regression technique (McIntyre et al. 1966; York 1966) which takes into account simultaneously the errors

Table 7. Fit parameters

Parameter	Sequence			
	I	II	III	IV
a_1	309 ± 22	180 ± 8	167 ± 30	175 ± 25
b_1^*	7.85 ± 0.69	19.43 ± 0.41	22.72 ± 1.72	20.32 ± 2.12
a_2	92.6 ± 9.3	59.4 ± 3.3	82.2 ± 14.9	66.0 ± 7.8
b_2	-0.15 ± 0.31	2.92 ± 0.19	2.64 ± 0.86	2.72 ± 0.68
a_3	13.2 ± 3.3	27.9 ± 3.3	119 ± 10	55.9 ± 4.1
b_3	0.33 ± 0.12	-0.11 ± 0.19	-4.90 ± 0.59	-2.29 ± 0.36
a_4	3.11 ± 0.21	2.95 ± 0.20	2.03 ± 0.18	2.57 ± 0.28
b_4	8.11 ± 0.65	10.89 ± 1.29	17.29 ± 1.43	14.13 ± 2.25
a_5	0.18 ± 0.04	0.45 ± 0.05	1.40 ± 0.20	0.98 ± 0.08
b_5	0.23 ± 0.12	-1.34 ± 0.30	-8.35 ± 1.48	-5.66 ± 0.66

*) All b_i values are in units $10^{-12} ergs\, cm^{-2}\, s^{-1}$

in both variables in contrast with the usual method which minimizes the distance along the y-axis only (see Feigelson & Babu (1992) for a review). The r.m.s. errors in the line and continuum fluxes were estimated for each sequence separately from the point-to-point scattering in the light curves in a 1.5 day window (the error bars shown in Fig. 8 are the mean errors for all sequences). The "doubly weighted" regression was also applied to the F(Hα)-F(Hβ) and F(He II)-F(Hβ) relationships, so we have five linear fits for each sequence:

$$F(\mathrm{H}\alpha) = a_1 F_\lambda(5120\text{Å}) + b_1$$
$$F(\mathrm{H}\beta) = a_2 F_\lambda(5120\text{Å}) + b_2$$
$$F(\mathrm{He\ II}\ \lambda4686) = a_3 F_\lambda(5120\text{Å}) + b_3$$
$$F(\mathrm{H}\alpha) = a_4 F(\mathrm{H}\beta) + b_4$$
$$F(\mathrm{He\ II}\ \lambda4686) = a_5 F(\mathrm{H}\beta) + b_5 \quad .$$

The time lag between the He II λ4686 and Hβ flux variations was taken from Table 6 as τ_{peak}(Balmer lines) $-\tau_{peak}$(He II λ4686); the fit parameters were calculated twice (by pairing the observed He II λ4686 fluxes with the interpolated Hβ fluxes and vice versa) and then averaged into the final values of a_5 and b_5. Note the F(Hα)-F(Hβ) relationship must be considered as the most reliable because its establishing requires no interpolation in light curves. The values of a_i, b_i are given in Table 7. The uncertainties in a_i, b_i have been taken as the largest of analytic (McIntyre et al. 1966) and jackknife (Feigelson & Babu 1992) computations. Together with Fig. 8, Table 7 evidences for the significant changes of both line-continuum and line-line relationships in NGC 4151 from one sequence to another.

The hatched rectangles in Fig. 8 show the allowed area for the constant contributions in the line and continuum fluxes. The lower limits for these contributions were discussed above (Sect.3.1) while the upper limits are simply the minimal fluxes ever observed. The latter are equal to 1.3×10^{-11}, 1.4×10^{-12},

and $4.7\times10^{-13}\,ergs\,cm^{-2}\,s^{-1}$ for the Hα, Hβ, and He II λ4686 lines respectively as estimated from the spectra of NGC 4151 in the 1984 minimum presented in Penston & Perez (1984), Filippenko & Sargent (1985), Ulrich et al. (1991), and to $1.8\times10^{-14}\,ergs\,cm^{-2}\,s^{-1}$ Å^{-1} for the optical continuum at 5120Å (Fig. 7). It is easy to see that the extrapolation of the first sequence passes through the hatched area while the extrapolation of any other sequence does not. Moreover, the extrapolations of sequences II, III, IV pass *above* the hatched area on the Hα-continuum and Hβ-continuum diagrams but *below* it on the He II-continuum diagram, so the link between the visible and ionizing continuum must be quite complicated.

4. Conclusion

Thus, the analysis of flux variability of NGC 4151 during the 8-year monitoring has revealed some features which contradict the simplest AGN paradigm where a single central source of the continuum emission has a steady relationship between the visible and ionizing continuum:

(1) each of the dependences of Hα, Hβ, and He II λ4686 emission-line fluxes on the optical continuum flux split into four sequences (Fig. 6,8) which cover different periods of observations and differ by most parameters of the line-continuum and line-line correlations including the time lag between the continuum and line variations (Tables 6,7);

(2) some sequences do not pass through the zero-point of both broad-line and non-thermal optical continuum fluxes, and the relative position of these sequences on the line-continuum diagram is quite different for the hydrogen and He II lines: the Hα-continuum and Hβ-continuum diagrams show that a significant hydrogen broad-line emission remains when the non-thermal optical continuum flux is extrapolated to zero while the He II λ4686 broad-line flux should disappear when the non-thermal optical continuum is essentially non-zero (Fig. 8);

(3) the transition time between two successive sequences ($\sim$ 100 days or less) is much shorter than the dynamical time scale for the BLR ($\sim$ several years), so the spatial redistribution of the line-emitting gas is obviously not the cause of the origin of sequences (and, hence, of the changes in the emission-line lag).

Of course, an analysis of variability of broad-line *profiles* will give us a lot of additional information about the processes taking place in the BLR of NGC 4151. Some intriguing features of the line profile variability pattern have been described already: at the second sequence, there were some wavelengths in the Hα line profile where the short-term variations of the line flux were correlated with the optical continuum variations while the slow systematic decrease of the line flux at these wavelengths was clearly anti-correlated with the systematic increase of the optical continuum (Sergeev et al. 1994). Another example is a slow growth of a component in the Hα and Hβ profiles due to which the sequences II-IV have stronger Hα and Hβ lines than the sequence I. Therefore, we leave the construction of any physical model for future papers where a comprehensive analysis of available observational data will be undertaken.

Acknowledgements. We are grateful to Drs. V.M. Lyutyi, N.I. Merkulova, and L.P. Metik for providing us the photometric data prior to publication. We thank Dr. S.Kaspi for measuring the mean [S II] flux in the spectra of NGC 4151 obtained in the Wise Observatory. This work was partially supported by the ESO C&EE grant A-01-057.

References

Antonucci, R.R.J., Cohen, R.D. 1983, ApJ 271, 564
Blandford, R.D., McKee, C.F. 1982, ApJ 255, 419
Clavel, J. et al. 1991, ApJ 366, 64
Dietrich, M. et al. 1993, ApJ 408, 416
Evans, I.N., Tsvetanov, Z., Kriss, G.A. et al., 1993, ApJ 417, 82
Fabrika, S.N. 1980a, Pisma v Astron. Zh. 6, 559
Fabrika, S.N. 1980b, Astron. Tsirk., No. 1109
Feigelson, E.D., Babu, G.J. 1992, ApJ 397, 55
Ferland, G.J., Korista, K.T., Peterson, B.M. 1990, ApJ 363, L21
Filippenko, A.V., Sargent, W.L.W. 1985, ApJS 57, 503
Gaskell, C.M., Peterson, B.M. 1987, ApJS 65, 1
Gill, T.R., Lloyd, C., Penston, M.V., Snijders, M.A.J. 1984, MNRAS 211, 31
Kaspi, S. et al. 1996, ApJ 470, 336
Kharitonov, A.V., Tereshchenko, V.M., Knyazeva, L.N. 1988, Spectrophotometric Catalogue of Stars, Science, Moscow
Korista, K.T. et al. 1995, ApJS 97, 285
Kriss, G.A. et al. 1995, ApJ 454, L7
Lyutyi, V.M. 1997, Astron. Zh., in preparation
Maoz, D., Netzer, H., Mazeh, T. et al., 1991, ApJ 367, 493
McIntyre, G.A., Brooks, C., Compston, W., Turek, A. 1966, J.Geophys.Res. 71, 5459
Merkulova, N.I., Metik, L.P. 1993, Izv.Krym.Astrofiz.Obs. 87, 136
Merkulova, N.I., Metik, L.P. 1995, Izv.Krym.Astrofiz.Obs. 90, 178
Moore, C.E. 1945, A Multiplet Table of Astrophysical Interest, Revised Ed. (Princeton, N.J.: Princeton University Observatory)
Penston, M.V. 1988, private communication
Penston, M.V., Perez, E. 1984, MNRAS 211, 33p
Perez, E., Gonzalez-Delgado, R., Tadhunter, C., Tsvetanov, Z. 1989, MNRAS 241, 31p
Peterson, B.M. 1993, PASP 105, 247
Peterson, B.M. et al. 1991, ApJ 368, 119
Phillips, I. 1978, ApJS 38, 187
Rakhimov, V.Yu. 1989, Byull. Inst. Astrofiz. AN Tadz. SSR No 78, 50
Reichert, G.A. et al. 1994, ApJ 425, 582
Sergeev, S.G. 1994, Astron. Zh. 71, 189
Sergeev, S.G., Malkov, Yu.F., Chuvaev, K.K., Pronik, V.I. 1994, in Reverberation Mapping of the Broad-Line Region in Active Galactic Nuclei, eds. Gondhalekar P. M., Horne K., Peterson B. M., ASP Conference Series 69, 199
Sergeev, S.G., Pronik, V.I., Malkov, Yu.F., Chuvaev, K.K. 1997, A&A 320, 405
Ulrich, M.-H., Boksenberg, A., Bromage, G.E. et al., 1991, ApJ 382, 483
Wanders, I., Peterson, B.M., Pogge, R.W., de Robertis, M.M., van Groningen, E. 1992, A&A 266, 72
Wanders, I. et al. 1993, A&A 269, 39
York, D. 1966, Canadian J.Phys. 44, 1079

This article was processed by the author using Springer-Verlag LaTeX A&A style file *L-AA* version 3.